Phosphate sequestration and recovery from eutrophication water by *in situ* magnesium phosphate formation

Fazhi Xie, Kang Song, Shixiong Geng and Lu Li

ABSTRACT

Phosphate removal from eutrophic lakes has caused wide concern in the world, while an effective process is still lacking. A novel synthetic magnesium carbonate with spherical flower-like structure (MCSF) was prepared. Its performance for phosphorus adsorption from a eutrophic lake by *in situ* magnesium phosphate formation was tested and characterized. The effect of initial phosphorus concentration, adsorption time, adsorption dose, temperature, ionic strength and pH on phosphorus adsorption by MCSF was investigated. Results showed that higher initial phosphorus concentration and longer adsorbing time could improve the adsorption capacity. The maximum sorption capacity was 143.27 mg/g under initial pH value 7.0. The phosphate adsorption process was fitted with the Langmuir isotherm model and pseudo-second-order model. Thermodynamic parameter values revealed that the sorption process at 298–318 K was spontaneous and endothermic. The X-ray diffraction (XRD) and X-ray photoelectron spectroscopy (XPS) characterization of MCSF revealed that electrostatic attraction and chemical conversion were the major contributors for phosphate adsorption. MCSF releases magnesium ions from its surface and rapidly combines with phosphate to form insoluble magnesium phosphate precipitate. The prepared MCSF has the potential to be used for the restoration of eutrophic lakes by removing phosphate with higher adsorption capacity.

Key words | chemical conversion, eutrophic lake, *in situ* adsorption, magnesium phosphate, phosphate removal

Fazhi Xie†
Shixiong Geng
School of Materials Science and Chemical Engineering,
Anhui Jianzhu University,
Hefei 230022,
China

Kang Song†
Shixiong Geng
Lu Li (corresponding author)
State Key Laboratory of Freshwater Ecology and Biotechnology,
Institute of Hydrobiology, Chinese Academy of Sciences,
Wuhan 430072,
China
E-mail: *lilu@ihb.ac.cn*

†These authors contributed equally.

HIGHLIGHTS

- A novel synthetic magnesium carbonate with spherical flower-like structure (MCSF) for phosphorus adsorption from a eutrophic lake by *in situ* magnesium phosphate formation was prepared.
- The maximum sorption capacity was 143.27 mg/g under initial pH value 7.0.
- The phosphate adsorption process was fitted with the Langmuir isotherm model and pseudo-second-order model.

doi: 10.2166/ws.2020.123

GRAPHICAL ABSTRACT

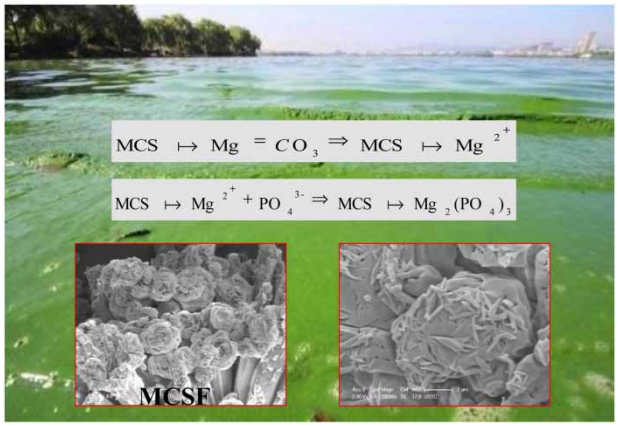

INTRODUCTION

Large amounts of wastewater discharge into surface water has led to lake eutrophication in China for a few decades (Le *et al.* 2010; Zhang *et al.* 2010; Herbeck *et al.* 2013; Wang *et al.* 2019), among which the existence of high phosphate concentration has been regarded as one of the most important factors that has caused lake eutrophication (Cai *et al.* 2010). Phosphate concentration over 0.02 mg/L could cause lake eutrophication. Municipal wastewater treatment plant effluent always contains phosphate concentration around 2 mg/L or even higher (Wang *et al.* 2015). Even though a stricter policy for external phosphate input into receiving water has been put into action, the release of phosphate from the sediments of lakes could also affect the lake trophic state (Zhao *et al.* 2010; Jiang *et al.* 2011; Ni *et al.* 2016; Xie *et al.* 2019). To control the phosphate in the surface water is of vital importance in lake trophic state control and water resource protection (Schindler *et al.* 2016).

Phosphate removal commonly includes biological process, chemical sedimentation, ion exchange, physical adsorption, membrane technology and so forth. The biological process is more suitable for high-concentration phosphate wastewater treatment, and the membrane technology is quite costly. Biological phosphate removal also has a low efficiency and high sludge-generation potential. The chemical sedimentation methods always generate a high quantity of metal-rich sludge, so a costly post-treatment is needed. Thus, the adsorption method, which could be used for low phosphate concentration situations, with low cost, less land use, being easy to control and with the phosphate recoverable, has aroused wide interest in this domain (Abeynaike *et al.* 2011; Zamparas *et al.* 2012; Li *et al.* 2016; Ahmed *et al.* 2019). Adsorption has been widely studied for phosphate removal from lakes. Wang *et al.* (2016) synthesized zeolite/hydrous lanthanum oxide composite by coal fly ash, which was highly efficient in capturing phosphate from eutrophic lake water. Lalley *et al.* (2016) reported that modified iron-oxide-based sorbents could be effective in adsorption of phosphate from lake water. The sorbent surface was modified with nanoparticles and enhanced the adsorption. Yang *et al.* (2020) found that aluminum-modified clay has high efficiency in removing the phosphorus from polluted lakes, and it is an effective passivator for internal phosphate remediation.

There are many materials that have been used as adsorbents for phosphate removal, including calcite, activated carbon, zeolite, metal and metal oxide (Awual *et al.* 2011; Song *et al.* 2011; Yadav *et al.* 2019). Most of those conventional adsorbents were not suitable for practical use due to lacking enough adsorption capacity or generating byproducts needing further treatment, limited their application for eutrophic lake restoration. Magnesium carbonate is a widely existing natural material, safe, low cost and

recoverable. It has been widely used in cosmetics and pharmaceutics, and this allows its safe application as an adsorbent to remove phosphate from eutrophic lakes (Lee & Chen 2015; Liang *et al.* 2017). Magnesium carbonate could slightly dissolve in water to release magnesium ions, and produce magnesium phosphate precipitation with the phosphate adsorbed. However, magnesium carbonate is not able to be used directly in its original form, due to its relatively low specific surface area. A suitable surface modification should be used to improve its specific surface area and its adsorption capacity.

This study prepared a novel synthetic magnesium carbonate with spherical flower-like structure (MCSF) for eutrophication restoration to adsorb phosphorus from a eutrophic lake by *in situ* magnesium phosphate formation. The prepared MCSF material and its adsorption mechanism was characterized.

MATERIALS AND METHODS

Materials

All chemicals used in this study were analytical pure purchased from Shanghai Kexi Chemical Co., Ltd, Shanghai, China.

MCSF preparation

Amounts of 1 M of sodium carbonate and magnesium chloride hexahydrate were weighed, and then dissolved in MilliQ water, separately. The sodium carbonate solution was slowly added to the magnesium chloride solution with stirring. Continuously stirred for 2 h, the solution was then washed with MilliQ water until free from chloride in the supernatant. Then, the product was filtrated and placed in a constant temperature oven at 50 °C for drying. The dried product was then ground and filtered through a molecular sieve. The material produced was magnesium carbonate with spherical flower-like structure (MCSF).

Adsorbent characterization

The phase identification analysis of the MCSF powder was carried out using an X'Pert PRO type X-ray diffractometer (XRD) (PANalytical BV, The Netherlands). Cu-Kα radiation ($\lambda = 1.5418$) was equipped, the tube voltage was 40 kV, tube current 40 mA and scanning speed 0.02°/s. A small amount of powder was tableted on a glass carrier and then subjected to an XRD test. The data were analyzed with XPSpeak 41 software. The grain size is calculated according to the Scherrer formula: $D = \mathrm{K}\lambda/\beta\cos\theta$, where D is the grain size (nm), K is the Scherrer constant: 0.89, λ is the X-ray wavelength: 0.15418 nm, β is the diffraction peak half-height width, and θ is the Bragg diffraction angle. The morphology of the powder was analyzed by Tecnai G220 transmission electron microscope (TEM) (FEI Company, The Netherlands). The acceleration voltage was 200 kV.

Equilibrium adsorption capacity test

Different volumes of phosphate solution and the same volume of MCSF were added in ten different centrifuge tubes and put in constant temperature water batch shaking for 12 h at temperature 25 °C. The solutions were centrifuged and their supernatants were analyzed by Phosphomolybdenum Blue spectrophotometry. The equilibrium adsorption capacity of the MCSF was calculated by Equation (1):

$$q_e = \frac{V(C_0 - C_e)}{m} \tag{1}$$

where q_e is the equilibrium adsorption capacity (mg/g), C_0 is the initial concentration of phosphate (mg/L), C_e is the phosphate equilibrium concentration (mg/L), V is the volume of phosphate solution, and m is the adsorbent mass (g).

Effect of ambient conditions on phosphate adsorption

The effect of ambient conditions on phosphate adsorption by MCSF was also conducted.

Adsorption time

Amounts of 37.5 mg MCSF and 15 mL phosphate solution (0.25 mg·P/mL) were weighed and put in three centrifuge tubes, respectively. The tubes were shaken on a constant

temperature shaker, and sampling was at 10, 20, 30, 40, 50, 60, 90, 120, 180, 240, 300, 360 min, respectively. The samples were then centrifuged at 400 rpm for five minutes, and filtrated with a 0.45 μm filter. The residue phosphate concentration was then measured and the adsorption capacity was calculated.

Temperature

Amounts of 37.5 mg MCSF and 15 mL phosphate solution (0.25 mg·P/mL) were weighed and put in three centrifuge tubes, respectively. The tubes were then put on a constant temperature shaker (20, 30 and 40 °C) and shaken for 300 min. Samples were taken after shaking was complete, centrifuged, filtrated and tested as for adsorption time.

The initial phosphate concentration

Amounts of 50 mg MCSF were weighed and put in ten centrifuge tubes, with initial phosphate concentrations 10, 30, 50, 70, 90, 110, 130, 150, 170 and 190 μg/mL, respectively. The tubes were then put on a constant temperature shaker for five hours, and then centrifuged, filtrated and tested as for adsorption time.

Ph

The pH of the phosphate solution (0.25 mg·P/mL) was adjusted to 3, 4, 5, 6, 7, 8, 9, 10 and 11 by 1 M NaOH and H_2SO_4 solution, respectively; 15 mL phosphate solution and 37.5 mg MCSF were then added to nine centrifuge tubes and shaken on a constant temperature shaker for 5 h, respectively. Samples were taken after shaking was completed, and then centrifuged, filtrated and tested as for adsorption time.

MCSF dosage

Amounts of 15 mL phosphate solution (0.25 mg·P/mL) and 15, 20, 25, 30, 40, 50, 60, 70 mg MCSF were added to eight centrifuge tubes and shaken on a constant temperature shaker for 5 h, respectively. Samples were taken after shaking was complete, centrifuged, filtrated and tested as for adsorption time.

The adsorption kinetics

An amount of 37.5 mg of MCSF was equilibrated with 15 mL of phosphate solution (250 mg/L) in a glass beaker (50 mL) at 25 °C for a fixed period of time (10, 20, 30, 40, 60, 90, 120, 180, 240, 300 and 360 min). Appropriate supernatant was filtered using a 0.45 μm filter and phosphate concentration was measured. The amount of phosphate adsorbed was calculated using Equation (1). The obtained experimental data were fitted by using the pseudo-first-order equation (Equation (2)) and the pseudo-second-order equation (Equation (3)) (Babaee *et al.* 2017):

$$\ln(q_e - q_t) = \ln q_e - k_1 t \tag{2}$$

$$\frac{t}{q_t} = \frac{1}{k_2 q_e^2} + \frac{1}{q_e} t \tag{3}$$

where q_t (mg/g) is the phosphate sorption capacity at time t, and k_1 (1/min) and k_2 (g/mg min) are the rate constant of pseudo-first-order adsorption and the equilibrium rate constant of pseudo-second-order adsorption.

Sorption isotherm and thermodynamics

Solutions of phosphate (50 mL) over the concentration range of 10–190 mg/L were maintained and shaken with MCSF (50 mg) at 288, 298, 308 and 318 K, respectively. The amounts of phosphate in the supernatant were determined. The sorption isotherm was described using Equations (4) and (5) as follows (Zhang *et al.* 2015):

$$\frac{C_e}{q_e} = \frac{C_e}{Q_{max}} + \frac{1}{b * Q_{max}} \tag{4}$$

$$\lg q_e = \frac{1}{n} \lg C_e + \lg K_F \tag{5}$$

where b is a Langmuir constant, Q_{max} is the theoretical maximum adsorption capacity, also known as monolayer coverage of the surface, K_F and n are characteristic constants of the system, where K_F is a measurement of adsorption capacity and $1/n$ of adsorption intensity.

The thermodynamic parameters of the adsorption process were determined from the experimental data obtained at 298 K, 308 K and 318 K using Equation (6), Equation

(7) and Equation (8) as follows (Lin & Zou 2017):

$$\Delta G^0 = -RT \ln K^0 \tag{6}$$

$$K_d = \frac{q_e}{C_e} \tag{7}$$

$$\ln K^0 = \frac{\Delta S^0}{R} - \frac{\Delta H^0}{RT} \tag{8}$$

where ΔG^0, ΔH^0 and ΔS^0 are Gibbs free energy change, enthalpy change and entropy change, respectively. K_d is the distribution coefficient for the adsorption, T is the absolute temperature, and R is the gas constant.

RESULTS AND DISCUSSION

Characterization of MCSF

The scanning electron microscope (SEM) image and energy dispersive X-ray (EDX) spectrum of the prepared MCSF before and after adsorption of phosphate are shown in Figure 1(a) and (b), respectively. As shown in Figure 1(a), the prepared MCSF has a spherical flower-like structure. It can be seen from Figure 1(b) that the adsorbent surface is aggregated with adsorbates to form an ingot-like structure. By comparing the EDX spectra of the phosphate unloaded and loaded adsorbents, it can be concluded that phosphate is adsorbed onto the MCSF.

Fourier transform infrared reflection (FTIR) spectra were used to determine the functional groups on the adsorbent surface and analyze the mechanism of phosphorus adsorption. The FTIR spectra of the adsorbents before and after phosphate adsorption is displayed in Figure 2. A new peak appeared at 1,039.18 cm^{-1} after phosphate adsorption, and two peaks increased obviously at 611.28 cm^{-1} and 3,442.94 cm^{-1}, respectively (Figure 2(b)). The strong double peaks that occurred at around 1,421.94 cm^{-1} and 1,514.1 cm^{-1} are the characteristic peaks of bicarbonate (Botha & Strydom 2003; Kirinovic *et al.* 2017). The spectra line that appeared at 1,667.39 cm^{-1} is the peak of H_2O (H-O-H) (deforming vibration), and the strong broad bands in the range of 2,500–4,000 cm^{-1} are the characteristic lines of H_2O (H-O-H) and OH (M-OH). The peak that appeared at 1,039.18 cm^{-1} after phosphorus adsorption indicated that the adsorption process may generate phosphate. Obviously higher and wider characteristic peaks were found at 661.28 cm^{-1}, 1,667.39 cm^{-1} and 3,442.94 cm^{-1} after adsorption, which could be attributed to the higher water content accumulated in the product after adsorption (the product of XRD is $Mg_3(PO_4)_2{\cdot}22H_2O$), leading to the broadening of the H_2O (H-O-H), OH (M-OH) and H_2O (i.e., H-O-H) (deformation vibration) characteristic lines (Ostrowski *et al.* 2014).

The thermogravimetric curve figure shows that the prepared MCSF remains stable at 378 K (Figure 3). From 378 K to 578 K, the rate of weight loss is 28.0%, which corresponds to the loss of $2H_2O$ from $MgCO_3{\cdot}3H_2O$ (the theoretical value is 26.0%) and a partial loss of another crystal water. Two crystal water were taken off one by one at low temperatures, indicated the presence of water molecules with two different binding capacities. The total weight loss from 378 K to 778 K is 39.2%, corresponding to the total loss of $3H_2O$ (the theoretical value is 39.0%) and this dehydration was carried out at higher and broader temperature ranges. This shows that the loss of water molecules is slow and difficult. Therefore, it can be considered that $2H_2O$

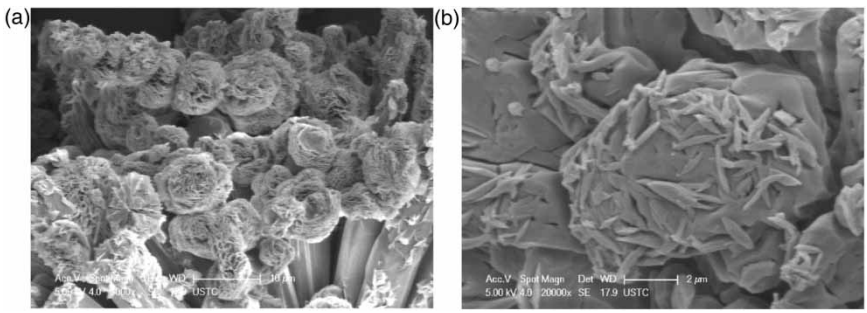

Figure 1 | SEM-EDX images of prepared adsorbent (a) before and (b) after adsorption of phosphorus ions (EDX: energy dispersive X-ray; SEM: scanning electron microscope).

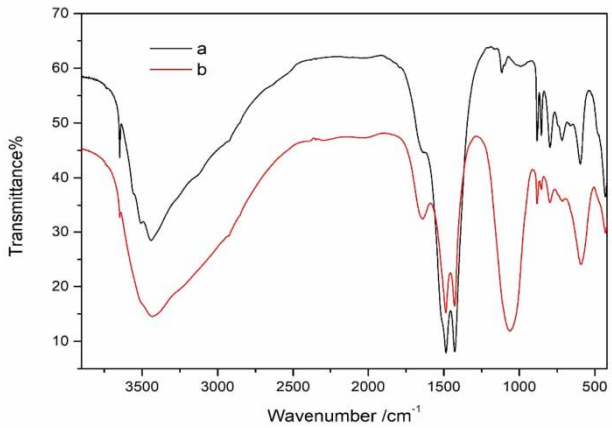

Figure 2 | FTIR spectra of the prepared adsorbent (a) without phosphate adsorption and (b) with phosphate adsorption.

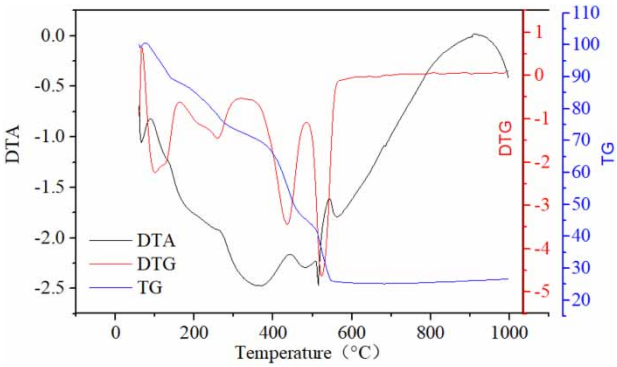

Figure 3 | Thermogravimetric curves.

molecules are the crystal water, and the other H_2O is structural water in $MgCO_3{\cdot}3H_2O$. From 778 K to 818 K, the rate of weight loss was 29.4% and a peak appeared at 800 K, indicated the process of MgO formation when anhydrous magnesium carbonate decomposed of CO_2 (the theoretical value is 31.8%). No weight loss was observed above 828 K and this shows that $MgCO_3$ was completely decomposed to MgO. This dehydration and thermal decomposition process is consistent with earlier studies (Han *et al.* 2014; Longo & Longo 2017).

The XRD patterns of the prepared MCSF before and after treatment with phosphate are shown in Figure 4. The sorbent composition before adsorption is $MgCO_3{\cdot}3H_2O$ and $Mg_3(PO_4)_2{\cdot}22H_2O$ after adsorption by XRD analysis. This indicated that the magnesium ion reacted with the phosphate in the solution during the adsorption process and magnesium phosphate precipitate was formed. High-resolution spectra of C1s can be deconvoluted into two peaks at about 284.67 eV and 289.5 eV. The band at 284.67 eV corresponds to the bonds from C-C and C-H; the peak at 289.5 eV indicates the presence of carbonate (Rheinheimer *et al.* 2017). The high-resolution spectrum of P2p has a peak at 133.5 eV corresponding to PO_4^{3-}, indicating the presence of PO_4^{3-} on the surface of MCSF. As can be seen from the XPS spectrum of Mg2p (Figure 5), a peak at 50.4 eV demonstrates the presence of $Mg_3(PO_4)_2$ (Felker & Sherwood 2002; Tsunakawa *et al.* 2017).

Performance of MCSF in ambient conditions

Effect of contact time

The removal efficiency of phosphate under different contact times was investigated at initial phosphate concentration 250 mg/L and adsorbent dosage 37.5 mg. The phosphate adsorption rate by MCSF kept increasing in the first 90 min, and started to stabilize after that (Figure S1, Supplementary Information). The adsorption capacity after 300 min increased by only 2.12% as compared with that of 90 min. It can be considered that the adsorption rate reached the maximum at 90 min, and the maximum adsorption capacity was 98.63 mg/g.

Effect of temperature

The effect of temperature on phosphate removal by MCSF was investigated. The adsorption efficiency of phosphate by MCSF was dramatically decreased with the increment of temperature (Figure S2). It may be due to the fact that the solubility of magnesium carbonate increases with the increasing of temperature. This resulted in a substantial reduction of magnesium carbonate that participated in the adsorption process. This could lead to the conclusion that the best temperature for the prepared MCSF in phosphate adsorption is 20 °C. More temperature conditions can be tested in future study to obtain an optimal adsorption temperature.

Effect of initial phosphate concentration

Phosphate with initial concentrations in the range of 10–190 mg/L was equilibrated using 50 mg adsorbent dose

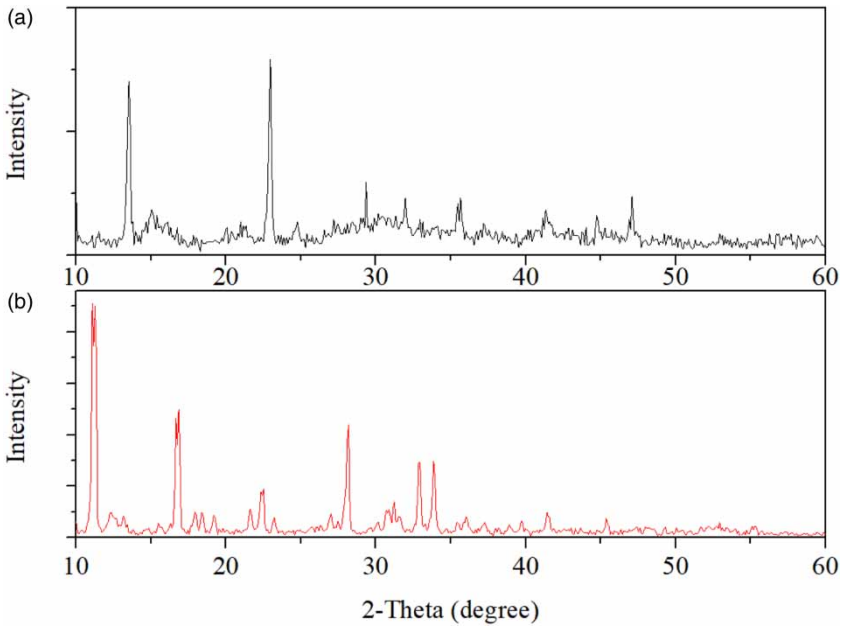

Figure 4 | XRD patterns of (a) MCSF, (b) MCSF after treatment with phosphate (XRD: X-ray diffraction).

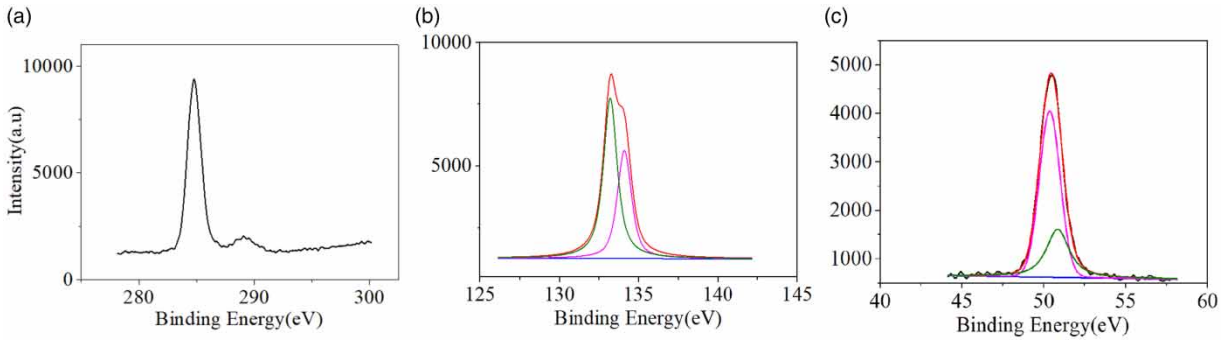

Figure 5 | XPS spectra of MCSF after treatment with phosphate: (a) C1s, (b) P2p and (c) Mg2p.

at 298 K. The phosphate ion equilibrium adsorption capacity increased from 9.81 to 144.13 mg/g, while the removal efficiency decreased from 98.1% to 75.86% when phosphate initial concentration increased from 10 to 190 mg/L (Figure S3). At low initial concentrations, the ratio of phosphate ions to the accessible active sites of adsorbent was low. Therefore, a higher phosphate removal efficiency occurred. The residual phosphate concentration in the solution increased with the increment of initial phosphate dosage, and this led to the increase of adsorption amount on the adsorbent. The adsorption capacity of prepared MCSF reached a relatively stable value of 144.13 mg/g at the initial phosphate concentration 190 mg/L, which could be regarded as the saturation adsorption point. This is much higher than other reported materials in the phosphate adsorption from eutrophic lakes.

Effect of pH

The effect of pH on adsorption capacity and removal efficiency of phosphate ions by the prepared MCSF was studied in the pH range 3.0–11.0 under adsorbent dosage 37.5 mg, initial phosphate concentration 250 mg/L and temperature 298 K. Results indicated that the maximum

phosphate removal by prepared MCSF occurred at pH 7.0. At low pH (3.0–7.0), the phosphate removal efficiency kept increasing due to the increment of protonated adsorbent surface. The high protonated adsorbent surface provided a strong electrostatic attraction between oxyanion and positively charged MCSF surface. The decrease of phosphate removal with the increase in pH 7.0–13.0 could be attributed to the increase in OH ions on the MCSF surface, which improved the repulsive force between negatively charged adsorbent surface and negatively charged phosphate ions.

Effect of adsorbent dosage

The effect of MCSF dosage on phosphate removal was also investigated. MCSF dosage from 1.5 to 6.0 g/L with contact time 300 min and initial phosphate concentration 250 mg/L was used. Results show that phosphorus removal increased with the increment of MCSF dosage. The removal rate started to reach a stable value after the MCSF dosage was over 5 g/L. Thus, an MCSF dosage of 5 g/L could be used as an optimal concentration for initial phosphate concentration 250 mg/L, and a removal rate over 94% could be achieved.

Adsorption kinetic study

The equilibrium adsorption capacity, pseudo-first-order and pseudo-second-order kinetic constant were calculated and are shown in Table 1. The correlation coefficients of 0.995, 0.999 and 0.999 were obtained through pseudo-second-order equation fitting (Figure 6), and indicated that the kinetic characteristics of phosphate adsorption by MCSF fitted to the model. The highest rate constant under the pseudo-second-order model was reached at the lowest temperature tested, 298 K, and this was consistent with the results of the temperature test. The highest adsorption capacity of prepared MCSF under the pseudo-second-order model was also found under the lowest temperature tested. This suggested that 298 K can be used as the optimal temperature during MCSF adsorption.

Table 1 | Kinetic parameters for the adsorption of PO_4 onto MCSF

		Pseudo-first-order kinetic model			Pseudo-second-order kinetic model		
T (K)	$q_{e,exp}$ (mg/g)	k_1 (h^{-1})	$q_{e,1}$ (mg/g)	R^2	k_2 (g/mg·h)	$q_{e,2}$ (mg/g)	R^2
298	99.0	0.0070	3.81	0.665	0.0065	104.38	0.995
308	94.0	0.0057	2.91	0.758	0.0026	95.06	0.999
318	89.5	0.0038	2.31	0.621	0.0046	89.61	0.999

Sorption isotherm and thermodynamics

The correlation of experimental data was also fitted to the Langmuir model and Freundlich model (Figure 7). The corresponding parameters were also calculated and are shown in Table 2. It can be seen from Figure 7 that the Langmuir model has significantly higher correlation than the Freundlich model, which indicates the homogeneous distribution of active sites on the adsorbent surface. The correlation coefficient R^2 of the Langmuir equation fitting was 0.995, 0.950 and 0.977 at 298, 308 and 318 K, and this is much higher than the value obtained from the Freundlich model. The highest adsorption capacity occurred at the temperature 298 K in both the Langmuir and Freundlich models, and this suggests that 298 K can be used as the best adsorption temperature.

The thermodynamic parameters (ΔG^0, $\Delta S^0$and ΔH^0) of the adsorption process were calculated with the obtained experimental data at several temperatures (Table 3). Gibbs free energy change (ΔG^0) during adsorption of PO_4 on MCSF has a more negative value at lower temperature, which demonstrates that the spontaneity of the adsorption process decreases with the increment of temperature. The positive value of entropy change (ΔS^0) implies an increase in the disorderliness of the solid–solution system, and indicates the contribution of structural changes that have taken place in adsorbate and adsorbent during the adsorption. A positive value of the standard enthalpy change (ΔH^0) indicates that the adsorption process is exothermic.

Sorption mechanism

The removal of phosphate by MCSF is not a simple adsorption process. The whole removal process involves (1) ionizing of $MgCO_3$ to magnesium ion, (2) magnesium ion generating $Mg_3(PO_4)_2$ *in situ*, (3) phosphate anion

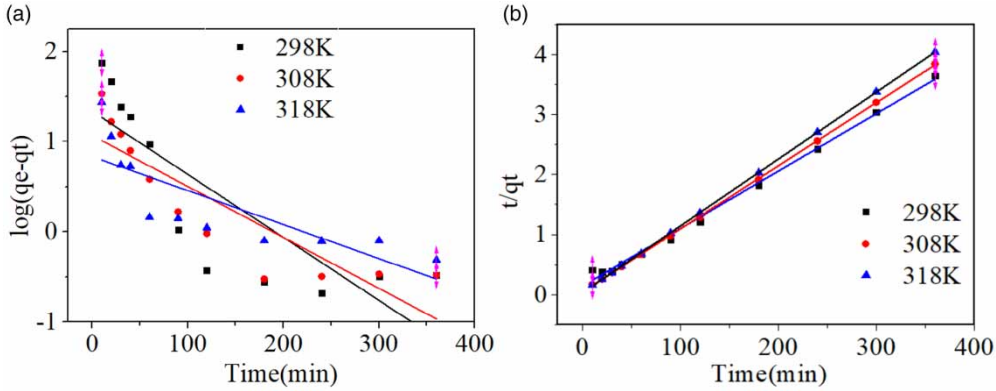

Figure 6 | The linear regression of the (a) pseudo-first-order kinetic model and (b) pseudo-second-order kinetic model.

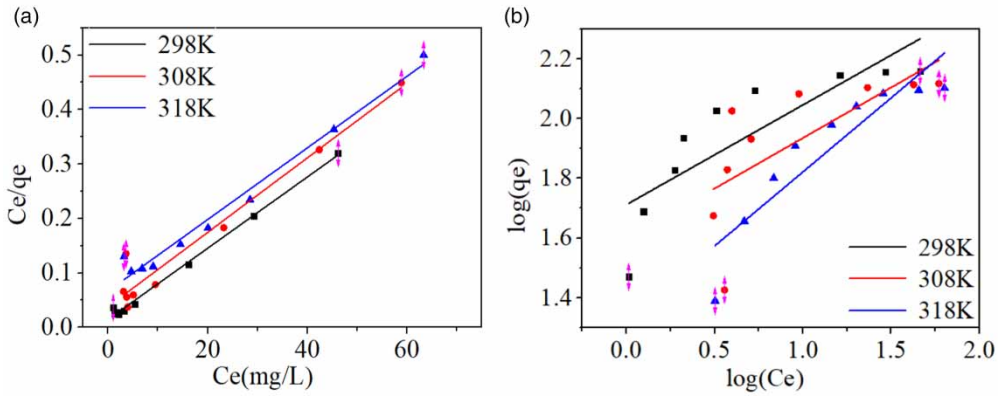

Figure 7 | Experimental data for PO_4 absorption fitted to the (a) Langmuir isotherm and (b) Freundlich isotherm.

adsorbing on the MCSF surface *in situ* to form a positively charged $MgCO_3$, (4) the reaction on the MCSF surface, phosphate adsorbing and converting to $Mg_3(PO_4)_2$. Thus, the proposed phosphate sorption mechanism by prepared MCSF is given as follows:

$$MCS \mapsto Mg = CO_3 \Rightarrow MCS \mapsto Mg^2+$$

$$MCS \mapsto Mg^2 + PO_4^{3-} \Rightarrow MCS \mapsto Mg_2(PO_4)_3$$

(MCS means the surface of magnesium carbonate)

The removal of phosphate by MCSF is not a simple adsorption process. The sorption process involves the magnesium ion release from MCSF in solution, the phosphate anion from solutions onto the adsorbing $MgCO_3$ through electrostatic attraction due to the presence of positive charge, and the *in situ* reaction between $MgCO_3$ and phosphate to conversion of the non-crystal-structure compound of $Mg_3(PO_4)_2$.

CONCLUSION

Magnesium carbonate with spherical flower-like structure (MCSF) was prepared and its phosphate adsorption performance was investigated. XRD characterization indicated that the composition of MCSF before adsorption was magnesium trihydrate and 22 hydrated magnesium phosphate after adsorption, which indicated that chemical adsorption occurred due to the precipitation of magnesium

Table 2 | The parameters for the Langmuir and Freundlich fitting of PO_4 adsorption on MCSF

	$T = 298$ K	$T = 308$ K	$T = 318$ K
Langmuir			
q_m (mg/g)	152.91	146.20	151.98
B (L/mg)	0.45	0.18	0.099
R^2	0.995	0.950	0.977
Freundlich			
K ($Fmg^{1-1/n}L^{1/n}/g$)	5.54	4.94	3.76
n	2.99	2.95	2.01
R^2	0.672	0.424	0.810

Table 3 | Thermodynamic parameters for the adsorption of PO_4 on MCSF

T (K)	lnK°	ΔG° (kJ/mol)	ΔS° (J/mol·K)	ΔH° (kJ/mol)
298	1.98	− 4.91	114.01	− 38.69
308	1.24	− 3.18		
318	1.00	− 2.64		

ions in magnesium carbonate combined with phosphate ions resulting in insoluble magnesium phosphate. The MCSF adsorption of phosphate has a highest adsorption capacity at pH 7, temperature 298 K. The maximum MCSF adsorption capacity can reach 143.27 mg/g. The adsorption process fitted well with the pseudo-second-order kinetic model and Langmuir model. The evaluated thermodynamic parameters such as ΔG, ΔH and ΔS revealed that the sorption process was spontaneous and exothermic in nature. The prepared MCSF has a high adsorption rate and is adapted to pH 7, temperature 298 K, and has a wide range of sources, low cost, and the potential to be developed as a highly efficient phosphate adsorbent in eutrophic lake restoration.

ACKNOWLEDGEMENT

The research was supported by Water Pollution Control and Treatment, National Science and Technology Major Project (Grant no. 2018ZX07208001), National Natural Science Foundation of China (Grant no. 41877344), China Postdoctoral Science Foundation (Grant no. 2019M652738). Dr. Kang Song acknowledges the supports from 100 Talents Program of Chinese Academy of Sciences (Y82Z08-1-401, Y75Z01-1-401).

SUPPLEMENTARY MATERIAL

The Supplementary Material for this paper is available online at https://dx.doi.org/10.2166/ws.2020.123.

REFERENCES

Abeynaike, A., Wang, L., Jones, M. I. & Patterson, D. A. 2011 Pyrolysed powdered mussel shells for eutrophication control: effect of particle size and powder concentration on the mechanism and extent of phosphate removal. *Asia-Pacific Journal of Chemical Engineering* **6** (2), 231–243.

Ahmed, S., Ashiq, M. N., Li, D., Tang, P., Leroux, F. & Feng, Y. 2019 Recent progress on adsorption materials for phosphate removal. *Recent Patents on Nanotechnology* **13** (1), 3–16.

Awual, M. R., Jyo, A., Ihara, T., Seko, N., Tamada, M. & Lim, K. T. 2011 Enhanced trace phosphate removal from water by zirconium (IV) loaded fibrous adsorbent. *Water Research* **45** (15), 4592–4600.

Babaee, Y., Mulligan, C. N. & Rahaman, M. S. 2017 Removal of arsenic (III) and arsenic (V) from aqueous solutions through adsorption by Fe/Cu nanoparticles. *Journal of Chemical Technology & Biotechnology* **93** (1), 63–71.

Botha, A. & Strydom, C. A. 2003 DTA and FTIR analysis of the rehydration of basic magnesium carbonate. *Journal of Thermal Analysis and Calorimetry* **71** (3), 987–996.

Cai, L. Y., Li, Y. & Zheng, Z. H. 2010 Temporal and spatial distribution of nitrogen and phosphorus of lake systems in China and their impact on eutrophication. *Earth and Environment* **38** (2), 235–241.

Felker, D. L. & Sherwood, P. M. A. 2002 Magnesium phosphate ($Mg_3(PO_4)_2$) by XPS. *Surface Science Spectra* **9** (1), 83–90.

Han, B., Qu, H., Niemi, H., Sha, Z. & Louhi-Kultanen, M. 2014 Mechanistic study of magnesium carbonate semibatch reactive crystallization with magnesium hydroxide and CO_2. *Industrial & Engineering Chemistry Research* **53** (30), 12077–12082.

Herbeck, L. S., Unger, D., Wu, Y. & Jennerjahn, T. C. 2013 Effluent, nutrient and organic matter export from shrimp and fish ponds causing eutrophication in coastal and back-reef waters of NE Hainan, tropical China. *Continental Shelf Research* **57**, 92–104.

Jiang, C., Hu, J., Huang, X., Li, C., Deng, J., Zhang, J. & Liu, F. 2011 Phosphorus speciation in sediments of Lake Hongfeng, China. *Chinese Journal of Oceanology and Limnology* **29** (1), 53–62.

Kirinovic, E., Leichtfuss, A. R., Navizaga, C., Zhang, H., Schuttlefield Christus, J. D. & Baltrusaitis, J. 2017

Spectroscopic and microscopic identification of the reaction products and intermediates during the struvite ($MgNH_4PO_4{\cdot}6H_2O$) formation from magnesium oxide (MgO) and magnesium carbonate ($MgCO_3$) microparticles. *ACS Sustainable Chemistry & Engineering* **5** (2), 1567–1577.

Lalley, J., Han, C., Li, X., Dionysiou, D. D. & Nadagouda, M. N. 2016 Phosphate adsorption using modified iron oxide-based sorbents in lake water: kinetics, equilibrium, and column tests. *Chemical Engineering Journal* **284**, 1386–1396.

Le, C., Zha, Y., Li, Y., Sun, D., Lu, H. & Yin, B. 2010 Eutrophication of lake waters in China: cost, causes, and control. *Environmental Management* **45** (4), 662–668.

Lee, D.-J. & Chen, Y.-Y. 2015 Magnesium carbonate precipitate strengthened aerobic granules. *Bioresource Technology* **183**, 136–140.

Li, M., Liu, J., Xu, Y. & Qian, G. 2016 Phosphate adsorption on metal oxides and metal hydroxides: a comparative review. *Environmental Reviews* **24** (3), 319–332.

Liang, W., Yin, Y., Wang, L., Chen, L. & Li, H. 2017 A new method of preparing anhydrous magnesium carbonate ($MgCO_3$) under high pressure and its thermal property. *Journal of Alloys and Compounds* **702**, 346–351.

Lin, L. & Zou, C. 2017 Kinetic and thermodynamic study of magnetic separable β-cyclodextrin inclusion complex with organic phosphoric acid applied to removal of Hg^{2+}. *Journal of Chemical & Engineering Data* **62** (2), 762–772.

Longo, G. M. & Longo, S. 2017 Thermal decomposition of $MgCO_3$ during the atmospheric entry of micrometeoroids. *International Journal of Astrobiology* **16** (4), 368–378.

Ni, Z., Wang, S. & Wang, Y. 2016 Characteristics of bioavailable organic phosphorus in sediment and its contribution to lake eutrophication in China. *Environmental Pollution* **219**, 537–544.

Ostrowski, N., Lee, B., Hong, D., Enick, P. N., Roy, A. & Kumta, P. N. 2014 Synthesis, osteoblast, and osteoclast viability of amorphous and crystalline tri-magnesium phosphate. *ACS Biomaterials Science & Engineering* **1** (1), 52–63.

Rheinheimer, V., Unluer, C., Liu, J., Ruan, S., Pan, J. & Monteiro, P. J. M. 2017 XPS study on the stability and transformation of hydrate and carbonate phases within MgO systems. *Materials* **10** (1), 75.

Schindler, D. W., Carpenter, S. R., Chapra, S. C., Hecky, R. E. & Orihel, D. M. 2016 Reducing phosphorus to curb lake eutrophication is a success. *Environmental Science & Technology* 50 (17), 8923–8929.

Song, X., Pan, Y., Wu, Q., Cheng, Z. & Ma, W. 2011 Phosphate removal from aqueous solutions by adsorption using ferric sludge. *Desalination* **280** (1–3), 384–390.

Tsunakawa, M., Shimada, Y., Nakamura, K., Kikuchi, K., Matsumura, T. & Ishizaki, T. 2017 Preparation and characteristics of phosphate conversion films on $AZ_{31}B$ magnesium alloy. *Keikinzoku/Journal of Japan Institute of Light Metals* **67** (10), 497–502.

Wang, X.-H., Wang, X., Huppes, G., Heijungs, R. & Ren, N.-Q. 2015 Environmental implications of increasingly stringent sewage discharge standards in municipal wastewater treatment plants: case study of a cool area of China. *Journal of Cleaner Production* **94**, 278–283.

Wang, Z., Fan, Y., Li, Y., Qu, F., Wu, D. & Kong, H. 2016 Synthesis of zeolite/hydrous lanthanum oxide composite from coal fly ash for efficient phosphate removal from lake water. *Microporous and Mesoporous Materials* **222**, 226–234.

Wang, J., Fu, Z., Qiao, H. & Liu, F. 2019 Assessment of eutrophication and water quality in the estuarine area of Lake Wuli, Lake Taihu, China. *Science of The Total Environment* **650**, 1392–1402.

Xie, F., Li, L., Song, K., Li, G., Wu, F. & Giesy, J. P. 2019 Characterization of phosphorus forms in a eutrophic lake, China. *Science of The Total Environment* **659**, 1437–1447.

Yadav, D., Kumar, P., Kapur, M. & Mondal, M. K. 2019 Phosphate removal from aqueous solutions by nano-alumina for the effective remediation of eutrophication. *Environmental Progress & Sustainable Energy* **38** (s1), S77–S85.

Yang, H., He, K., Lu, D., Wang, J., Xu, D., Jin, Z., Yang, M. & Chen, J. 2020 Removal of phosphate by aluminum-modified clay in a heavily polluted lake, Southwest China: effectiveness and ecological risks. *Science of The Total Environment* **705**, 135850.

Zamparas, M., Gianni, A., Stathi, P., Deligiannakis, Y. & Zacharias, I. 2012 Removal of phosphate from natural waters using innovative modified bentonites. *Applied Clay Science* **62–63**, 101–106.

Zhang, Q., Zhang, Z., Teng, J., Huang, H., Peng, Q., Jiao, T., Hou, L. & Li, B. 2015 Highly efficient phosphate sequestration in aqueous solutions using nanomagnesium hydroxide modified polystyrene materials. *Industrial & Engineering Chemistry Research* **54** (11), 2940–2949.

Zhang, X. J., Chen, C., Ding, J. Q., Hou, A., Li, Y., Niu, Z. B., Su, X. Y., Xu, Y. J. & Laws, E. A. 2010 The 2007 water crisis in Wuxi, China: analysis of the origin. *Journal of Hazardous Materials* **182** (1–3), 130–135.

Zhao, Y., Deng, X., Zhan, J., Xi, B. & Lu, Q. 2010 Progress on preventing and controlling strategies of Lake Eutrophication in China. *Environmental Science & Technology (China)* **33** (3), 92–98.

First received 2 October 2019; accepted in revised form 28 May 2020. Available online 12 June 2020